Broadband selective excitation of topological bound states in the continuum within two-dimensional supersymmetric photonic lattices

Xuanyu Liu,[1,*] Xuhu Han,[2,*] Wange Song,[1,†] Yuying Wang,[2] Zhiyuan Lin,[1] Shengjie Wu,[1] Lijing Zhong,[3,‡] Shining Zhu,[1] Jianrong Qiu,[2,§] and Tao Li[1,‖]

[1]*National Laboratory of Solid State Microstructures, Key Laboratory of Intelligent Optical Sensing and Manipulations, Jiangsu Key Laboratory of Artificial Functional Materials, College of Engineering and Applied Sciences, Nanjing University, Nanjing 210093, China*

[2]*State Key Laboratory of Extreme Photonics and Instrumentation, College of Optical Science and Engineering, Zhejiang University, Hangzhou 310027, China*

[3]*Institute of Light+X Science and Technology, College of Information Science and Engineering, Ningbo University, Ningbo 315211, China*

(Received 7 November 2024; revised 17 January 2025; accepted 10 February 2025; published 21 February 2025)

Bound states in the continuum (BICs), which are localized waves within a continuous spectrum of radiating waves, have garnered considerable attention due to their counterintuitive physical properties. However, selectively exciting these bound states from the continuum remains challenging because of their degenerate eigenenergy. In this work, we propose a method to accurately excite high-order topological BICs (TBICs) using supersymmetric (SUSY) structures. By adiabatically transforming the SUSY partner to the original lattice, TBICs can be perfectly excited with simple single-site excitation. We experimentally verify our strategy in photonic waveguides at telecommunication wavelengths, demonstrating efficient excitation and the existence of TBICs across a broadband. Our work highlights the superior capability of SUSY in regulating optical BIC modes, suggesting possibilities for exploring BICs in higher-dimensional lattices.

DOI: 10.1103/PhysRevB.111.075427

I. INTRODUCTION

Bound states in the continuum (BICs), which are localized states that have eigenenergy (i.e., eigenfrequency) in the continuum of extended states, have been extensively studied in various systems [1–14]. Due to their counterintuitive physical properties, BICs have garnered widespread interest, leading to explorations of their generation mechanisms [8,15–19] and possible applications [8,15,20]. However, these studies require high-quality bound modes, yet research on the precise excitation of BICs remains lacking. Take the topological bound states in the continuum (TBICs) in higher-dimensional topological insulators (HOTIs) as an example (the mechanism of *separable BICs* [21–23] causes the energy levels of localized higher-dimensional topological states to merge into the bulk band); although the TBICs enrich the conventional theory of topological states and provide topological protection to BICs, they encounter significant excitation challenges due to their degeneracy with bulk states. To better demonstrate their properties, the perfect excitation of TBICs becomes especially important, which facilitates the observation of BIC-related topological effects and enhances the efficiency of associated applications, such as high-quality BIC laser emission [24–26], high-efficiency low-loss waveguiding [27,28], and so on. Previous approaches include adding non-Hermitian losses to the bulk [29], directly utilizing zero-mode sources to observe BICs [30] and breaking the symmetry protection using nonlinear control [31–33]. These methods either substantially disrupt BICs or have difficulties in avoiding the excitation of extended states, leading to inefficiency. It is of significant importance to find a general method to fully and exclusively excite the TBIC without strongly disturbing its eigenproperties.

Supersymmetry is a mathematic transformation originally developed in quantum field theory [34–38]; it was also applied to optics [39,40], which enables flexible designs on the optical potential while generally preserving the eigenenergy spectrum. The supersymmetric (SUSY) method has already been applied in optical devices, such as in single-mode laser arrays [41–43], mode conversion [40,44], and light routing [45,46]. It is noteworthy that SUSY transformations have been applied to transport photonic modes in structures that have continuous refractive index distribution [45,46], but research on applying SUSY to control modes in higher-dimensional topological lattices remains lacking. Due to its precise mode manipulation capabilities, the SUSY principle would provide a feasible route to accurately select TBICs modes in the continuum, thereby achieving perfect mode excitation.

In this paper, we theoretically propose and experimentally demonstrate a supersymmetric (SUSY) route for TBIC excitation in photonic waveguides. Specifically, we design a SUSY partner based on the original high-order topological lattice that supports nontrivial corner-bound states. It is found that through an appropriate adiabatic connection of topological structure and its SUSY partner, the single-site input

*These authors contributed equally to this work.
†Contact author: songwange@nju.edu.cn
‡Contact author: zhonglijing@nbu.edu.cn
§Contact author: qjr@zju.edu.cn
‖Contact author: taoli@nju.edu.cn

waveguide mode in the SUSY partner can evolve robustly into the corner-bound states of interest, which are further verified by experiments in waveguide arrays inscribed in glass samples using direct femtosecond laser writing technology [47–51]. Interestingly, this SUSY approach enables an efficiently selective excitation of TBIC across a broadband, thereby greatly advancing the exploration of the physical mechanisms and application potentials of BICs. It is noteworthy that compared to previous SUSY-based photonic devices, this work achieved broadband selective excitation of high-dimensional BIC modes.

II. BOUND STATES IN THE CONTINUUM IN TWO-DIMENSIONAL SSH LATTICE

We demonstrate our design principle based on the topological corner-bound states in the two-dimensional Su-Schrieffer-Heeger (2D SSH) model [52–54] (see Fig. 1), which can be implemented in the photonic waveguides [55]. In the one-dimensional SSH model, topological properties are commonly characterized by the Zak phase [56]. In the 2D SSH model, the 2D Zak phase can be defined, which undergoes a shift from (0, 0) to (π, π) when transitioning from a topologically trivial phase to a nontrivial one. The transition of the 2D Zak phase characterizes the high-order topological phase, which is protected by C_{4v} group symmetry [52]. The Hamiltonian for the tight-binding 2D SSH model can be represented as the Kronecker sum of the Hamiltonians of two one-dimensional (1D) SSH models [57,58]. The SSH model is characterized by two sublattices with staggered weak (strong) couplings κ_1 (κ_2), and can host zero-energy edge-bound states if the outermost coupling is weak. The edge states have nonzero projections in one of the sublattices due to chiral symmetry, and their amplitudes decay according to a common ratio of $q = -\kappa_1/\kappa_2$ in an interval sublattice. The corner-bound states in the 2D SSH model are correspondingly localized at the corner with weak couplings on both sides [30,31,53] [see Fig. 1(b)]. In Fig. 1(c), we calculated the eigenvalues of the 2D SSH model as a function of κ_1/κ_2. It is evident that there are several degenerate modes persistently present at the zero-energy level. When $\kappa_1 > \kappa_2$, the system resides in a topologically trivial phase where there are no localized corner states. In contrast, when $\kappa_1 < \kappa_2$, the corner states enter the band, thereby indicating the presence of TBICs. For simplicity, we selected a 5 × 5-site system at the corner to perform the SUSY operation, which is adequate for efficiently exciting the TBICs because the energy distribution of the corner states has already decayed to a negligible level outside of this subsystem (see Supplemental Material [59]; also see [30,51,53,60–62]). The energy spectrum of the 2D SSH lattice is shown in Fig. 1(a). Due to chiral symmetry and lattice symmetry, five degenerate zero modes form a continuum, within which the topological corner state resides. Considering the symmetry along the x and y directions, there are three distinct zero modes in the system, with only one being a BIC [30,31,53] [see Fig. 1(d)]. Note that due to the joint protection of chiral symmetry and C_{4v} symmetry, this TBIC mode does not interfere with the other two modes in the continuum [29,30,52].

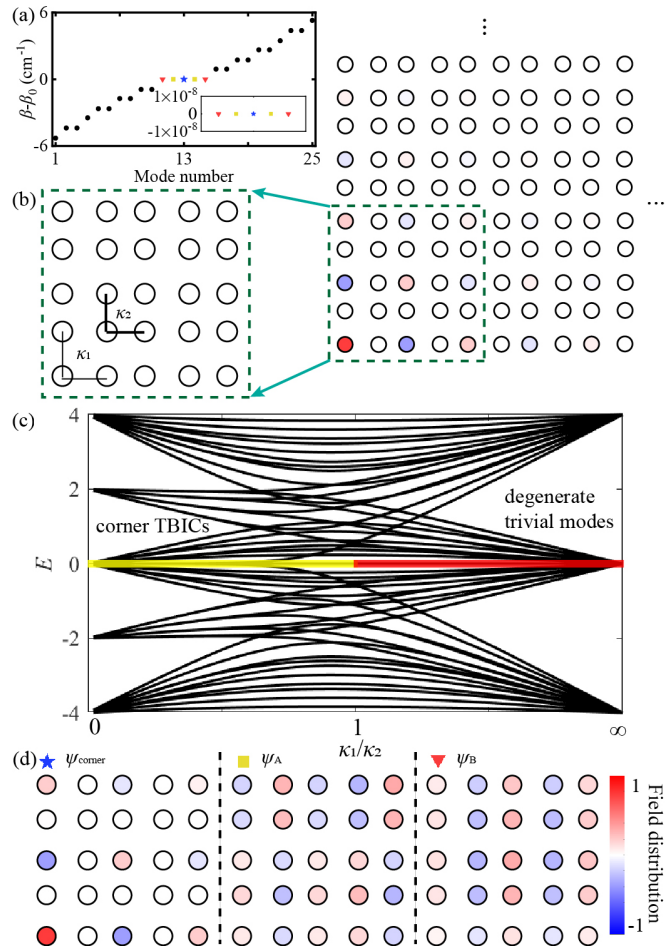

FIG. 1. (a) Calculated eigenvalues of the tight-binding 2D SSH lattice. A TBIC (blue pentagram) emerges within the bulk bands. (b) Schematics of the topological nontrivial 2D SSH lattice with weak couplings κ_1 and strong couplings κ_2. A 5 × 5-site system at the corner is selected to perform the SUSY operation. (c) Calculated eigenvalues of the 10 × 10-site 2D SSH lattice as a function of κ_1/κ_2,where $\kappa_1 + \kappa_2 = 2$. The regions of corner TBICs and degenerate trivial modes are highlighted with yellow and red regions on the zero-mode bands. (d) The eigenmode profiles of three different types of zero-energy modes (ψ_{corner}, ψ_A, ψ_B) of which only one is corner bound. The total site number $N^2 = 25$. $\kappa_1 = 1$ cm^{-1}, $\kappa_2 = 2$ cm^{-1}.

III. EXCITATION OF CORNER-BOUND STATES BY SUSY

One-dimensional discrete supersymmetry (1D DSUSY) transformations [40,44,60,63,64] can generate two supersymmetric partner Hamiltonians $H^{(1)}$ and $H^{(2)}$ with different but isospectral 1D structures. If supersymmetry is unbroken, $H^{(2)}$ will display an isolated site whose eigenvalue of the supported mode exactly corresponds to the one that desired to be excited [59]. Due to the presence of energy level degeneracy in 2D lattices, a direct application of the 1D DSUSY transformation to the 2D Hamiltonian is usually unfeasible. Fortunately, Qiao *et al.*, in their study of single-mode laser arrays using the DSUSY method, innovatively extended the DSUSY transformation to a higher-dimensional lattice [43]. This work demonstrates that because of the separability of the 2D SSH model, it is possible to perform 1D DSUSY transformations

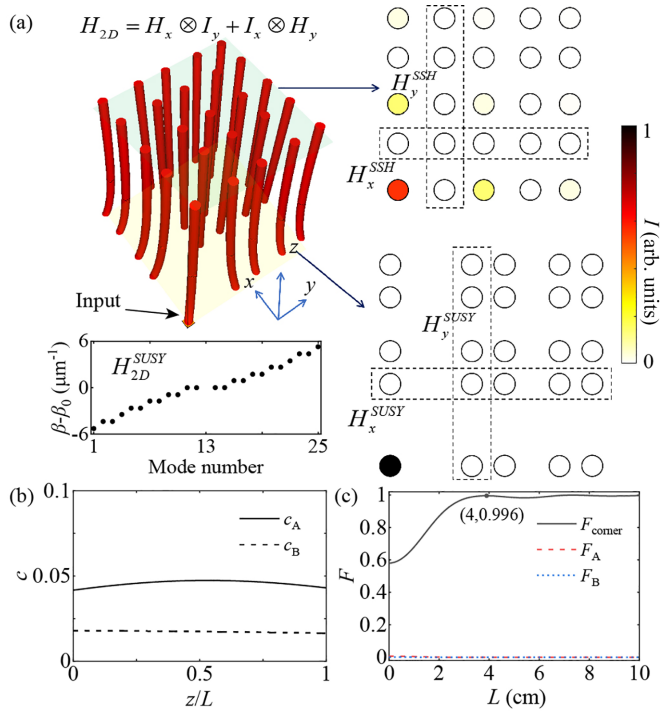

FIG. 2. (a) Left panel: Schematics of the designed waveguide lattice that is adiabatically varying from SUSY ($z = 0$) to the 2D SSH ($z = L$) lattices. L is the length of the waveguides. Calculated eigenvalues of the SUSY lattice, where the TBIC ψ_{corner} is isolated. Right panel: Normalized intensity profiles of the corner zero-energy states in the SUSY lattice ($z = 0$) and 2D SSH ($z = L$) lattices. (b) Adiabatic parameter c as a function of propagation length z/L. $L =$ 4 cm. (c) Fidelity of the zero modes as a function of waveguide length L. $\kappa_1 = 1$ cm^{-1}, $\kappa_2 = 2$ cm^{-1}.

separately on its 1D sublattices in two directions x and y [Fig. 2(a)], thereby achieving the 2D DSUSY transformation [43],

$$\begin{aligned} H_{2\mathrm{D}}^{\mathrm{SSH}} &= H_x^{\mathrm{SSH}} \otimes I_y + I_x \otimes H_y^{\mathrm{SSH}}, \\ H_{2\mathrm{D},mn}^{\mathrm{SUSY}} &= H_{x,m}^{\mathrm{SUSY}} \otimes I_y + I_x \otimes H_{y,n}^{\mathrm{SUSY}}, \\ H_x^{\mathrm{SSH}} - \lambda_{x,m} I &= Q_x R_x, \quad H_{x,m}^{\mathrm{SUSY}} = R_x Q_x + \lambda_{x,m} I, \\ H_y^{\mathrm{SSH}} - \lambda_{y,n} I &= Q_y R_y, \quad H_{y,n}^{\mathrm{SUSY}} = R_y Q_y + \lambda_{y,n} I, \end{aligned} \tag{1}$$

where I is the identity matrix, Q is an orthogonal matrix, and R is an upper triangular matrix. H_x^{SSH}, H_y^{SSH} and $H_{x,m}^{\mathrm{SUSY}}$, $H_{y,n}^{\mathrm{SUSY}}$ denote the Hamiltonians of the 1D SSH model and its SUSY partner, where x and y denote the two 1D sublattices derived by the direct sum decomposition; m and n ($m, n = -2, -1, 0, 1, 2$) represent the mode numbers of the selected eigenmodes in the two directions. $\lambda_{x(y),m(n)}$ is the mth (nth) mode's eigenvalue in the 1D SSH Hamiltonian $H_{x(y)}$. $H_{2\mathrm{D}}^{\mathrm{SSH}}$ and $H_{2\mathrm{D}}^{\mathrm{SUSY}}$ refer to the Hamiltonians of the 2D SSH model and its SUSY partner. The QR factorization can be achieved using the *Givens rotation method* [60,65], which is one feasible method to achieve the SUSY transformation. The eigenvalues of the SUSY partner Hamiltonian obtained through this transformation remain invariant. However, the matrix representation and the distribution of eigenstates undergo changes. The selected mode $|\psi_{m,n}>$ is isolated in a single site, while the distribution of other modes experiences relatively minimal alterations. Through the aforementioned transformation, one can obtain the SUSY partner Hamiltonian corresponding to the 2D SSH model. The physical system (photonic waveguides in this work) corresponding to this Hamiltonian is referred to as the SUSY lattice. Note that there are multiple possible SUSY lattices, among which we choose the one whose Hamiltonian closely matches the original 2D SSH Hamiltonian [59].

Our model is implemented in the 2D photonic waveguide lattices, as seen in the schematics shown in the left panel of Fig. 2(a). The input end of the waveguide array is a SUSY lattice of which the eigenvalues are identical to the original 2D SSH lattice [Fig. 1(a)] except for the corner state. An isolated waveguide serves as the input port and the output end is the 2D SSH lattice. A slowly varying waveguide array connects the two ends, ensuring adiabatic evolution of the single-site-input optical field in the waveguide. At the input end (i.e., SUSY lattice), the original TBIC ($m, n = 0$) with complicated mode distribution is projected into a single waveguide mode [bottom in right panel in Fig. 2(a)]. While the excitation of the transformed TBIC is straightforward, evolving this single-site state into the TBIC of interest requires the input SUSY lattice to adiabatically transform into the 2D SSH lattice at the output end. Therefore, the waveguide array should vary slowly to ensure that the input photonic state remains on the TBIC band throughout its evolution, with minimal crosstalk with other modes in the continuum. Consequently, the target TBIC is faithfully reconstructed at the output end [upper right panel in Fig. 2(a)], completing the selective excitation process.

Here we assume the following modulation on the waveguide lattice: $H_{2\mathrm{D}}(z) = g(z)H_{2\mathrm{D}}^{\mathrm{SSH}} + [1-g(z)]H_{2\mathrm{D}}^{\mathrm{SUSY}}$, where the modulation function $g(z)$ should satisfy the condition $g(z)\in$[0 [1],] and $g(0) = 0$, $g(L) = 1$. Through this layout, we connect the SUSY structure with the original structure, enabling a smooth transition between the two lattices $H_{2\mathrm{D}}(0) = H_{2\mathrm{D}}^{\mathrm{SUSY}}$ and $H_{2\mathrm{D}}(L) = H_{2\mathrm{D}}^{\mathrm{SSH}}$. For simplicity, we choose a linear modulation $g(z) = z/L$, with unchanged $g'(z)$ to make sure the SUSY array undergoes uniform variations at a steady rate. To ensure the input zero mode evolves along the BIC energy level, the structure parameters should be slowly varied. Here, we define an *adiabatic parameter c* to measure the adiabaticity [66],

$$\begin{aligned} c(z) &= \sqrt{c_x(z)c_y(z)}, \\ c_x(z) &= \left| \frac{\langle \phi_{x,m}(z) | \frac{\partial}{\partial z} | \phi_{x,n}(z) \rangle}{\lambda_{x,m} - \lambda_{x,n}} \right|, \\ c_y(z) &= \left| \frac{\langle \phi_{y,m}(z) | \frac{\partial}{\partial z} | \phi_{y,n}(z) \rangle}{\lambda_{y,m} - \lambda_{y,n}} \right|, \end{aligned} \tag{2}$$

where the subscripts x and y are used to differentiate the eigenvalues and eigenvectors belonging to a specific 1D SSH Hamiltonian, while the subscripts m and n distinguish different eigenvalues and eigenstates within that Hamiltonian. Therefore, the numerator and denominator of c_x and c_y

represent the strength of the *Berry connection* and the energy gap between bands of the 1D SSH model m and n, respectively. From the results of the 1D adiabatic parameters, we can get the trend of crosstalk between the two 2D modes $|\psi_{i,m}\rangle = |\phi_{x,i}\rangle \otimes |\phi_{y,m}\rangle$ and $|\psi_{j,n}\rangle = |\phi_{x,j}\rangle \otimes |\phi_{y,n}\rangle$, where the numerator and denominator of c_x and c_y represent the strength of the *Berry connection* and the energy gap between bands of the 1D SSH model m and n, respectively. A small value of an adiabatic parameter ($c \ll 1$) indicates the adiabatic condition can be satisfied. Figure 2(b) shows the adiabatic parameter between the corner-bound mode band $\psi_{\text{corner}} = |\psi_{0,0}\rangle = |\phi_{x,0}\rangle \otimes |\phi_{y,0}\rangle$ and other two types of zero-mode bands in the continuum $\psi_{\text{A}} = |\psi_{\pm1,\mp1}\rangle = |\phi_{x,\pm1}\rangle \otimes |\phi_{y,\mp1}\rangle$, $\psi_B = |\psi_{\pm2,\mp2}\rangle = |\phi_{x,\pm2}\rangle \otimes |\phi_{y,\mp2}\rangle$ of the SUSY array. It is found that within SUSY structures, corner-bound states are remarkably difficult to crosstalk with other zero modes in the continuum, showcasing excellent satisfaction of adiabatic conditions. To characterize the quality of the output BICs (i.e., the efficiency of topological state pumps), we define the fidelity $F = |\langle\Phi_0|\phi(L)\rangle|^2$, where Φ_0 is the exact eigenmode of the 2D SSH corner-bound states we aim to produce and $\Phi(L)$ is the actual output state. As shown in Fig. 2(c), the calculated fidelity is larger than 99% for $L > 4$ cm, where the adiabaticity can be well preserved. In contrast, the fidelity without the SUSY structure (i.e., with direct single-site input to the SSH array) is only 58% under the same conditions [59]. Additionally, the fidelity of other zero modes in the continuum is effectively suppressed throughout the entire evolution process (<0.01), demonstrating the ability of SUSY to selectively excite BICs.

IV. EXPERIMENTAL RESULTS

We experimentally verify the TBIC excitation in a 2D evanescently coupled waveguide array. The single-mode-cutoff condition for single-mode guidance in circular waveguides (fibers) is given by

$$V = 2\pi \frac{r}{\lambda_0}\text{NA} \approx 2\pi \frac{r}{\lambda_0} n\sqrt{2\Delta n} \leqslant 2.405, \tag{3}$$

where r is the waveguide radius, λ_0 is the wavelength of input light, NA is the numerical aperture of the waveguide, n is the refractive index, and Δn is the refractive index contrast. These parameters have been provided in Fig. 3. Under these structural parameters, as illustrated in Fig. 3(a), it is evident that the single-mode condition is satisfied for the wavelength range under investigation. Figure 3(b) shows the coupling coefficient as the function of gap distance, from which the exponential correspondence between the coupling coefficient and the gap distance $\kappa(d) = \kappa_0 \exp(-\gamma d)$ can be fitted ($\kappa_0 = 100\ \text{cm}^{-1}$, $\gamma = 0.2\ \mu\text{m}^{-1}$). Two gap distances for our SSH waveguide array can be selected, i.e., $d_1 = 23.03\ \mu$m for $\kappa_1 = 1\ \text{cm}^{-1}$ and $d_2 = 19.54\ \mu$m for $\kappa_2 = 2\ \text{cm}^{-1}$. Note that as the wavelength increases, the V parameter decreases, which is equivalent to reducing the effective numerical aperture while keeping the wavelength constant. This signifies a weaker confinement capability of the waveguides, resulting in smaller values for the fitting parameters κ_0 and γ. With the designed structural parameters, the complete view of the glass sample with the laser-written waveguide array is shown in Fig. 3(c). The colored stripes indicate positions. Each transparent stripe in the sample represents a waveguide array (single-input SSH array or SUSY-input array). The scale of each array is ∼100 μm, with the waveguides extending over a total length of 5 cm.

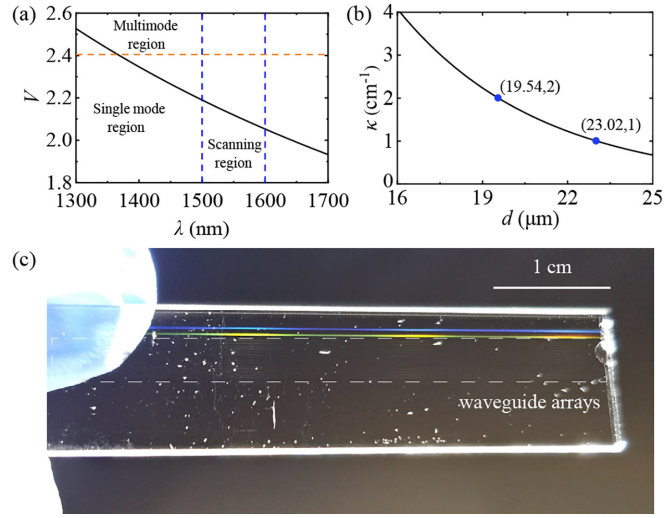

FIG. 3. (a) The V parameter of circular waveguide (fiber) as a function of wavelength for the step index waveguide with radius $r \sim 3.2$ μm, refractive index $n \sim 1.5$, refractive index contrast $\Delta n \sim 10^{-3}$. Each single-mode waveguide supports only one fundamental LP11 mode at $\lambda = 1550$ nm. The waveguides are fabricated in glass (Corning Eagle XG) using femtosecond-laser (1030 nm) writing. (b) Coupling coefficient as a function of gap distance with the wavelength $\lambda = 1550$ nm. (c) Glass sample with femtosecond-laser-written waveguide arrays.

In the experiment, a femtosecond laser was focused into the glass to fabricate the sample, which was moved controllably to write the waveguide structures, with the input end face shown in Fig. 4(a). In the left panel, the waveguide array begins with a SUSY lattice at the input end, which undergoes adiabatic evolution to transform into the SSH lattice at the output end. In contrast, the right panel consistently maintains the SSH lattice in a straight waveguide array. The light was input into the waveguides by focusing the laser ($\lambda = 1550$ nm) through a fiber. The output of the waveguides was collected by a microscope objective and subsequently measured by a near-infrared beam profiler (see Methods for details of measurement). The extracted output intensity of the 2D SSH lattice with SUSY design is displayed in Fig. 4(b), which agrees well with the theoretical values [Fig. 4(d)], confirming that the adiabatically varying SUSY array can almost realize the exact eigenmode of corner-bound states. As a comparison, the normalized output intensity of the single waveguide input case shows relatively poor locality and indicates more deviations from the BICs to the degenerate zero modes and bulk modes[(Figs. 4(c) and 4(e)].

Moreover, it is expected that the SUSY design can work in a broadband manner, similar to the broadband results demonstrated by Yim *et al.* in continuous SUSY structures [46]. As the wavelength changes, the coupling coefficients of H_{SUSY} and H_{SSH} undergo varying degrees of alteration, leading to a situation where the SUSY conditions are no longer strictly

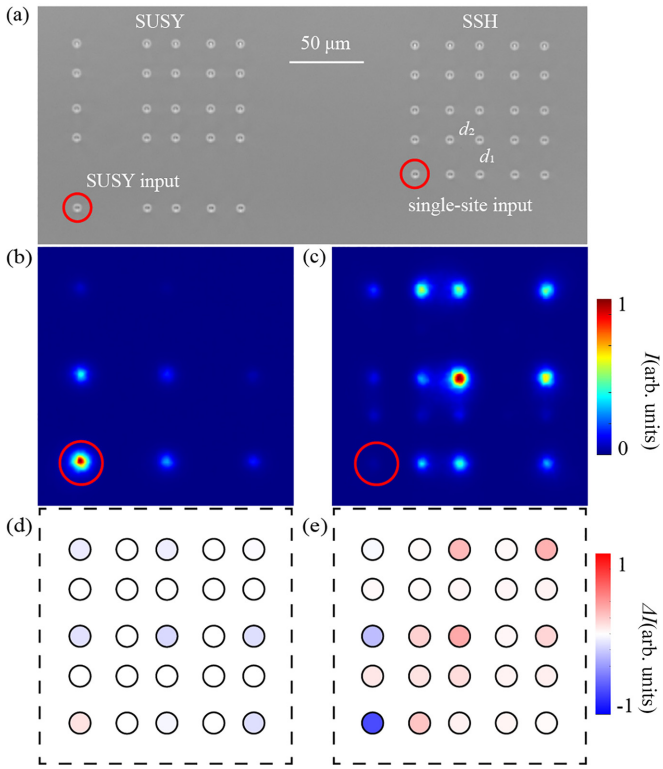

FIG. 4. (a) The waveguide cross sections of the SUSY input and single-site input 2D SSH lattice at the input end. The gaps $d_{1(2)} = 23.03(19.54)$ μm correspond to coupling coefficients $\kappa_{1(2)} = 1\ (2)\ \mathrm{cm}^{-1}$. (b–e) Experimentally recorded output intensity profiles (I) with (b) SUSY-input and (c) single-site input structure, and deviations from the exact zero modes (ΔI, bottom panels) with (d) SUSY-input and (e) single-site input structure.

satisfied. However, the SUSY structure can still preserve mode correspondence, effectively preventing crosstalk during light transmission. Here, we provide the experimentally measured output intensities of different wavelengths (1500–1600 nm). As shown in Fig. 5, the output modes with SUSY design exhibit similar intensity distributions across a wide wavelength range. In contrast, the output intensities with single-site input all deviate from the BIC distributions. This is because for SUSY waveguides, changes in wavelength only alter the coupling coefficients of the output 2D SSH lattice and introduce a perturbation to the modulation function $g(z)$. Both of these changes do not break the adiabatic conditions of the SUSY structures and the topological properties of the topological 2D SSH lattice, hence exerting minimal impact on the output distribution [59]. We anticipate that these excellent results of the SUSY arrays are also robust against structural perturbations. In fact, due to the fulfillment of the adiabatic condition, our SUSY design still performs well even under a higher disorder strength [59].

In practical systems, the next-nearest-neighbor (NNN) coupling in the 2D SSH model is usually inevitable, so we further considered the effects of the NNN couplings and demonstrated its influence on the SUSY transformation and the BIC excitations [59].

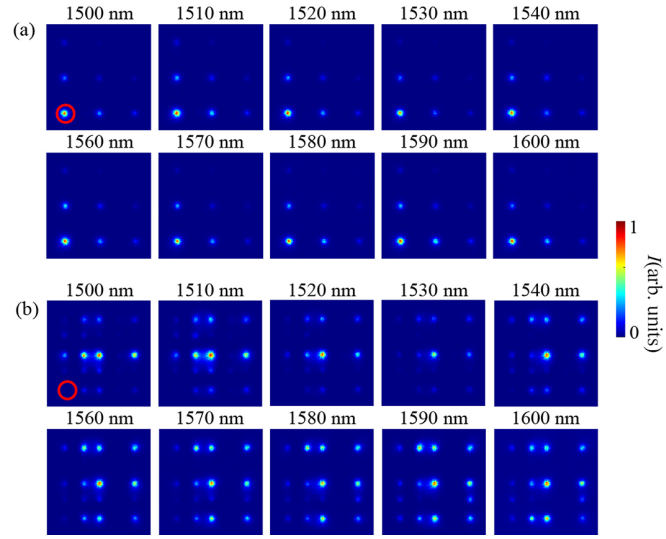

FIG. 5. Wavelength-dependent behavior of the output of 2D SSH array with (a) SUSY-input and (b) single-site input for 1500–1600 nm.

V. ACCELERATING THE EVOLUTION OF TBICs BY INVERSE DESIGN

In the previous text, we employed a linear coupling function $g(z)$ to ensure that the system satisfies adiabatic conditions when L is sufficiently large, which inevitably leads to a large device footprint (e.g., 4 cm in Fig. 4). Indeed, there can be more choices for $g(z)$ that significantly reduce the required L for perfect excitation of BICs. Inspired by the shortcut to the adiabaticity (STA) technique proposed in quantum physics to speed up the quantum state transfer [67–70], here we employ a similar accelerating process by inverse-design approaches [71,72] that can produce the same final state in a shorter length. Specifically, if the input and output of the waveguides are fixed and the length L is determined, the fidelity would be solely determined by a generalized modulation function $g(z)$,

$$g(z) = g_{\mathrm{lin}} + g_f = \frac{z}{L} + \sum_{n=1}^{N_c} a(n) \sin\left(\frac{2n\pi z}{L}\right), \qquad (4)$$

where g_f is a half-range Fourier series and N_c is a cutoff number. Note here $g(z)$ should be centrally symmetric about the point (L/2, 1/2) as required by the symmetry of the excitation process. Using computational inverse-design approaches [64,71,72], we achieve the optimal fidelity F_{max} for different lengths under the constraint of $g(z) \in [0\ [1],]$, as shown in Fig. 6(a). It is evident that the optimized SUSY arrays can significantly reduce the required length for the same fidelity (e.g., from 4 to 2.2 cm for $F \sim 0.99$). In this situation, the adiabaticity is destroyed and the zero modes are allowed to couple to other bulk modes. However, they eventually return to the zero-energy band and reproduce the desired topological zero modes [Fig. 6(b)]. Figure 6(c) shows more results about the proportion of zero modes p_0. It can be observed that as the waveguide array length L increases, the light field propagation in the inverse-design structures increasingly approaches adiabatic evolution. Figure 6(d) illustrates that as L increases,

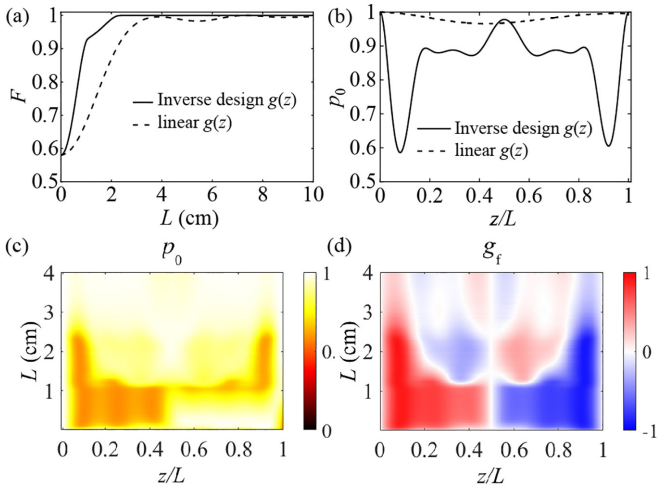

FIG. 6. (a) Fidelity of the zero modes for increasing device length. (b) Proportion of the zero mode (p_0) as a function of propagation length z/L [$L = 2.2$ cm for optimized $g(z)$ and 4 cm for linear $g(z)$]. (c) The profiles of $p_0(z/L)$ for different waveguide lengths L. (d) The profiles of g_f (z/L) for different waveguide lengths L.

the shape of $g(z)$ tends toward linearity, indicating improved satisfaction of adiabatic conditions.

VI. DISCUSSION

It is noteworthy that the SUSY principle has been employed for the excitation of celebrated topological edge states, exhibiting excellent broadband performance and robustness [64]. However, compared to conventional topological states, the TBICs in higher-order topological insulators feature level degeneracy and complex mode distributions, rendering them more challenging to accurately excite and utilize. Here, we extend the SUSY principle to higher dimensions and successfully excite the accurate TBICs of interest. Notably, the topological phase of the 2D SSH model remains unchanged with variations in wavelength, ensuring the existence of TBIC in a broadband manner [59,73]. Our SUSY design enables efficient excitation of such broadband TBIC modes. Additionally, the SUSY approaches also show flexibilities in selectively exciting all preferred eigenmodes, including the degenerate bulk zero modes [59].

In conclusion, we have exploited the topological zero-mode evolution in adiabatic SUSY structure to perfectly excite the eigenmode of a corner-bound state. We apply SUSY transformations to the 2D SSH lattices hosting topological BICs. Adiabatically connecting the topological array and its SUSY partner enables the single-site zero mode to evolve robustly into the BICs of interest in broadband. The experimental results in femtosecond-laser-writing waveguide arrays are fully consistent with our expectations. The selective excitation of TBICs implies unique possibilities in practical applications. For example, the excited TBICs exhibit a light-guiding mechanism distinct from refractive index guidance, which can be utilized for topological light transport in low-index materials [30]. TBICs in 2D SSH lattices do not require band-gap protection, but instead are topologically and symmetry protected, thereby demonstrating excellent broadband performance. Our SUSY principle avoids the unwanted modes in the continuum, thereby enhancing the quality of light, which is crucial for possible high-precision optical quantum state manipulation [74] and large-scale photonic integrations [73,75].

ACKNOWLEDGMENTS

The authors acknowledge the financial support from The National Key R&D Program of China (Grant No. 2022YFA1404301), the National Natural Science Foundation of China (Grants No. 12204233, No. 12174186, No. 62325504, No. 62288101, and No. 92250304). T.L. acknowledges the support from Dengfeng Project B of Nanjing University.

[1] H. Friedrich and D. Wintgen, Interfering resonances and bound states in the continuum, Phys. Rev. A **32**, 3231 (1985).
[2] H. Friedrich and D. Wintgen, Physical realization of bound states in the continuum, Phys. Rev. A **31**, 3964 (1985).
[3] D. C. Marinica, A. G. Borisov, and S. V. Shabanov, Bound states in the continuum in photonics, Phys. Rev. Lett. **100**, 183902 (2008).
[4] Y. Plotnik, O. Peleg, F. Dreisow, M. Heinrich, S. Nolte, A. Szameit, and M. Segev, Experimental observation of optical bound states in the continuum, Phys. Rev. Lett. **107**, 183901 (2011).
[5] C. W. Hsu, B. Zhen, J. Lee, S.-L. Chua, S. G. Johnson, J. D. Joannopoulos, and M. Soljačić, Observation of trapped light within the radiation continuum, Nature (London) **499**, 188 (2013).
[6] S. Weimann, Y. Xu, R. Keil, A. E. Miroshnichenko, A. Tünnermann, S. Nolte, A. A. Sukhorukov, A. Szameit, and Y. S. Kivshar, Compact surface Fano states embedded in the continuum of waveguide arrays, Phys. Rev. Lett. **111**, 240403 (2013).
[7] Y. Yang, C. Peng, Y. Liang, Z. Li, and S. Noda, Analytical perspective for bound states in the continuum in photonic crystal slabs, Phys. Rev. Lett. **113**, 037401 (2014).
[8] C. W. Hsu, B. Zhen, A. D. Stone, J. D. Joannopoulos, and M. Soljačić, Bound states in the continuum, Nat. Rev. Mater. **1**, 16048 (2016).
[9] H. Zhou, B. Zhen, C. W. Hsu, O. D. Miller, S. G. Johnson, J. D. Joannopoulos, and M. Soljačić, Perfect single-sided radiation and absorption without mirrors, Optica **3**, 1079 (2016).
[10] J. Gomis-Bresco, D. Artigas, and L. Torner, Anisotropy-induced photonic bound states in the continuum, Nat. Photonics **11**, 232 (2017).
[11] A. Kodigala, T. Lepetit, Q. Gu, B. Bahari, Y. Fainman, and B. Kanté, Lasing action from photonic bound states in continuum, Nature (London) **541**, 196 (2017).
[12] M. Minkov, I. A. D. Williamson, M. Xiao, and S. Fan, Zero-index bound states in the continuum, Phys. Rev. Lett. **121**, 263901 (2018).
[13] A. Cerjan, C. W. Hsu, and M. C. Rechtsman, Bound states in the continuum through environmental design, Phys. Rev. Lett. **123**, 023902 (2019).

[14] A. Overvig, N. Yu, and A. Alù, Chiral quasi-bound states in the continuum, Phys. Rev. Lett. **126**, 073001 (2021).

[15] J. Wang *et al.*, Optical bound states in the continuum in periodic structures: Mechanisms, effects, and applications, Photonics Insights **3**, R01 (2024).

[16] P. Hu, J. Wang, Q. Jiang, J. Wang, L. Shi, D. Han, Z. Q. Zhang, C. T. Chan, and J. Zi, Global phase diagram of bound states in the continuum, Optica **9**, 1353 (2022).

[17] B. Zhen, C. W. Hsu, L. Lu, A. D. Stone, and M. Soljačić, Topological nature of optical bound states in the continuum, Phys. Rev. Lett. **113**, 257401 (2014).

[18] K. Koshelev, G. Favraud, A. Bogdanov, Y. Kivshar, and A. Fratalocchi, Nonradiating photonics with resonant dielectric nanostructures, Nanophotonics **8**, 725 (2019).

[19] M. Kang, S. Zhang, M. Xiao, and H. Xu, Merging bound states in the continuum at off-high symmetry points, Phys. Rev. Lett. **126**, 117402 (2021).

[20] M. Kang, T. Liu, C. T. Chan, and M. Xiao, Applications of bound states in the continuum in photonics, Nat. Rev. Phys. **5**, 659 (2023).

[21] V. M. Apalkov and M. E. Raikh, Strongly localized mode at the intersection of the phase slips in a photonic crystal without band gap, Phys. Rev. Lett. **90**, 253901 (2003).

[22] N. Prodanović, V. Milanović, Z. Ikonić, D. Indjin, and P. Harrison, Bound states in continuum: Quantum dots in a quantum well, Phys. Lett. A **377**, 2177 (2013).

[23] N. Rivera, C. W. Hsu, B. Zhen, H. Buljan, J. D. Joannopoulos, and M. Soljačić, Controlling directionality and dimensionality of radiation by perturbing separable bound states in the continuum, Sci. Rep. **6**, 33394 (2016).

[24] M.-S. Hwang, H.-C. Lee, K.-H. Kim, K.-Y. Jeong, S.-H. Kwon, K. Koshelev, Y. Kivshar, and H.-G. Park, Ultralow-threshold laser using super-bound states in the continuum, Nat. Commun. **12**, 4135 (2021).

[25] Y. Yu, A. Sakanas, A. R. Zali, E. Semenova, K. Yvind, and J. Mørk, Ultra-coherent Fano laser based on a bound state in the continuum, Nat. Photonics **15**, 758 (2021).

[26] H. Zhong, Y. Yu, Z. Zheng, Z. Ding, X. Zhao, J. Yang, Y. Wei, Y. Chen, and S. Yu, Ultra-low threshold continuous-wave quantum dot mini-BIC lasers, Light. Sci. Appl. **12**, 100 (2023).

[27] T. Dong *et al.*, Ultra-low-loss on-chip zero-index materials, Light. Sci. Appl. **10**, 10 (2021).

[28] T. Dong *et al.*, Low-loss nanoscale zero-index metawaveguides and metadevices, Optica **11**, 799 (2024).

[29] W. A. Benalcazar and A. Cerjan, Bound states in the continuum of higher-order topological insulators, Phys. Rev. B **101**, 161116(R) (2020).

[30] A. Cerjan, M. Jürgensen, W. A. Benalcazar, S. Mukherjee, and M. C. Rechtsman, Observation of a higher-order topological bound state in the continuum, Phys. Rev. Lett. **125**, 213901 (2020).

[31] Z. Hu *et al.*, Nonlinear control of photonic higher-order topological bound states in the continuum, Light. Sci. Appl. **10**, 164 (2021).

[32] M. S. Kirsch *et al.*, Nonlinear second-order photonic topological insulators, Nat. Phys. **17**, 995 (2021).

[33] A. A. Arkhipova *et al.*, Observation of π solitons in oscillating waveguide arrays, Sci. Bull. **68**, 2017 (2023).

[34] A. Neveu and J. H. Schwarz, Factorizable dual model of pions, Nucl. Phys. B **31**, 86 (1971).

[35] P. Ramond, Dual theory for free fermions, Phys. Rev. D **3**, 2415 (1971).

[36] D. V. Volkov and V. P. Akulov, Is the neutrino a goldstone particle? Phys. Lett. B **46**, 109 (1973).

[37] J. Wess and B. Zumino, Supergauge transformations in four dimensions, Nucl. Phys. B **70**, 39 (1974).

[38] E. Witten, Dynamical breaking of supersymmetry, Nucl. Phys. B **188**, 513 (1981).

[39] M.-A. Miri, M. Heinrich, and D. N. Christodoulides, Supersymmetry-generated complex optical potentials with real spectra, Phys. Rev. A **87**, 043819 (2013).

[40] M. A. Miri, M. Heinrich, R. El-Ganainy, and D. N. Christodoulides, Supersymmetric optical structures, Phys. Rev. Lett. **110**, 233902 (2013).

[41] M. P. Hokmabadi, N. S. Nye, R. El-Ganainy, D. N. Christodoulides, and M. Khajavikhan, Supersymmetric laser arrays, Science **363**, 623 (2019).

[42] B. Midya, H. Zhao, X. Qiao, P. Miao, W. Walasik, Z. Zhang, N. M. Litchinitser, and L. Feng, Supersymmetric microring laser arrays, Photonics Res. **7**, 363 (2019).

[43] X. Qiao *et al.*, Higher-dimensional supersymmetric microlaser arrays, Science **372**, 403 (2021).

[44] M. Heinrich, M. A. Miri, S. Stutzer, R. El-Ganainy, S. Nolte, A. Szameit, and D. N. Christodoulides, Supersymmetric mode converters, Nat. Commun. **5**, 3698 (2014).

[45] W. Walasik, N. Chandra, B. Midya, L. Feng, and N. M. Litchinitser, Mode-sorter design using continuous supersymmetric transformation, Opt. Express **27**, 22429 (2019).

[46] J. Yim, N. Chandra, X. Feng, Z. Gao, S. Wu, T. Wu, H. Zhao, N. M. Litchinitser, and L. Feng, Broadband continuous supersymmetric transformation: A new paradigm for transformation optics, eLight **2**, 16 (2022).

[47] Y. Yang *et al.*, Low-loss skimming waveguides with controllable mode leakage for on-chip saturable absorbers, Nanophotonics **12**, 3069 (2023).

[48] L. Zhong, Y. Wang, D. Tan, and J. Qiu, Toward 3D integration of highly see-through photonic circuits in glass, Laser Photonics Rev. **17**, 2200767 (2023).

[49] D. Chen *et al.*, 3D Laser writing of low-loss cross-section-variable type-I optical waveguide passive/active integrated devices in single crystals, Adv. Mater. **36**, e2404493 (2024).

[50] X. Han, Y. Wang, J. Hu, L. Zhong, and J. Qiu, Laser printing of large-area conformal 3D photonic circuits in glass, Laser Photonics Rev. **18**, 2400060 (2024).

[51] Y. Wang *et al.*, Precise mode control of laser-written waveguides for broadband, low-dispersion 3D integrated optics, Light. Sci. Appl. **13**, 130 (2024).

[52] F. Liu and K. Wakabayashi, Novel topological phase with a zero Berry curvature, Phys. Rev. Lett. **118**, 076803 (2017).

[53] B.-Y. Xie, G.-X. Su, H.-F. Wang, H. Su, X.-P. Shen, P. Zhan, M.-H. Lu, Z.-L. Wang, and Y.-F. Chen, Visualization of higher-order topological insulating phases in two-dimensional dielectric photonic crystals, Phys. Rev. Lett. **122**, 233903 (2019).

[54] X.-D. Chen, W.-M. Deng, F.-L. Shi, F.-L. Zhao, M. Chen, and J.-W. Dong, Direct observation of corner states in second-order topological photonic crystal slabs, Phys. Rev. Lett. **122**, 233902 (2019).

[55] A. Yariv, Coupled-mode theory for guided-wave optics, IEEE J. Quantum Electron. **9**, 919 (1973).

[56] J. Zak, Berry's phase for energy bands in solids, Phys. Rev. Lett. **62**, 2747 (1989).

[57] W. P. Su, J. R. Schrieffer, and A. J. Heeger, Solitons in polyacetylene, Phys. Rev. Lett. **42**, 1698 (1979).

[58] A. J. Heeger, S. Kivelson, J. R. Schrieffer, and W. P. Su, Solitons in conducting polymers, Rev. Mod. Phys. **60**, 781 (1988).

[59] See Supplemental Mateiral at http://link.aps.org/supplemental/10.1103/PhysRevB.111.075427 for discussion about SUSY transformation of 1D SSH model, broadband TBICs in the 2D SSH model, excitation of bulk modes by SUSY design, influence of the system sizes, effects of next-neighbor coupling, robustness analyses of the SUSY structure, and which includes Refs. [30,51,53,60–62].

[60] G. Queraltó, M. Kremer, L. J. Maczewsky, M. Heinrich, J. Mompart, V. Ahufinger, and A. Szameit, Topological state engineering via supersymmetric transformations, Commun. Phys. **3**, 49 (2020).

[61] J. Wu *et al.*, Higher-order topological polariton corner state lasing, Sci. Adv. **9**, eadg4322 (2023).

[62] M. Li, D. Zhirihin, M. Gorlach, X. Ni, D. Filonov, A. Slobozhanyuk, A. Alù, and A. B. Khanikaev, Higher-order topological states in photonic kagome crystals with long-range interactions, Nat. Photonics **14**, 89 (2020).

[63] D. Viedma, G. Queralto, J. Mompart, and V. Ahufinger, High-efficiency topological pumping with discrete supersymmetry transformations, Opt. Express **30**, 23531 (2022).

[64] X. Liu, Z. Lin, W. Song, J. Sun, C. Huang, S. Wu, X. Xiao, H. Xin, S. Zhu, and T. Li, Perfect excitation of topological states by supersymmetric waveguides, Phys. Rev. Lett. **132**, 016601 (2024).

[65] L. Hogben, *Handbook of Linear Algebra*, 2nd ed. (Chapman & Hall/CRC, Boca Raton, FL, 2013).

[66] M. Born and V. Fock, Beweis des adiabatensatzes, Z. Med. Phys. **51**, 165 (1928).

[67] X. Chen, I. Lizuain, A. Ruschhaupt, D. Guéry-Odelin, and J. G. Muga, Shortcut to adiabatic passage in two- and three-level atoms, Phys. Rev. Lett. **105**, 123003 (2010).

[68] D. Guéry-Odelin, A. Ruschhaupt, A. Kiely, E. Torrontegui, S. Martínez-Garaot, and J. G. Muga, Shortcuts to adiabaticity: Concepts, methods, and applications, Rev. Mod. Phys. **91**, 045001 (2019).

[69] N. N. Hegade, K. Paul, Y. Ding, M. Sanz, F. Albarrán-Arriagada, E. Solano, and X. Chen, Shortcuts to adiabaticity in digitized adiabatic quantum computing, Phys. Rev. Appl. **15**, 024038 (2021).

[70] Z. Yin, C. Li, J. Allcock, Y. Zheng, X. Gu, M. Dai, S. Zhang, and S. An, Shortcuts to adiabaticity for open systems in circuit quantum electrodynamics, Nat. Commun. **13**, 188 (2022).

[71] S. Molesky, Z. Lin, A. Y. Piggott, W. Jin, J. Vucković, and A. W. Rodriguez, Inverse design in nanophotonics, Nat. Photonics **12**, 659 (2018).

[72] L. Ma, J. Li, Z. Liu, Y. Zhang, N. Zhang, S. Zheng, and C. Lu, Intelligent algorithms: New avenues for designing nanophotonic devices [Invited], Chin. Opt. Lett. **19**, 011301 (2021).

[73] W. Song, W. Sun, C. Chen, Q. Song, S. Xiao, S. Zhu, and T. Li, Robust and broadband optical coupling by topological waveguide arrays, Laser Photonics Rev. **14**, 1900193 (2020).

[74] A. Blanco-Redondo, B. Bell, D. Oren, B. J. Eggleton, and M. Segev, Topological protection of biphoton states, Science **362**, 568 (2018).

[75] A. Blanco-Redondo, I. Andonegui, M. J. Collins, G. Harari, Y. Lumer, M. C. Rechtsman, B. J. Eggleton, and M. Segev, Topological optical waveguiding in silicon and the transition between topological and trivial defect states, Phys. Rev. Lett. **116**, 163901 (2016).